

# Meshed High-Impedance Matching Network-Free Rectenna Optimized for Additive Manufacturing

MAHMOUD WAGIH<sup>1</sup> (Graduate Student Member, IEEE), ALEX S. WEDDELL<sup>1</sup> (Member, IEEE),  
AND STEVE BEEBY<sup>1</sup> (Senior Member, IEEE)

School of Electronics and Computer Science, University of Southampton, Southampton SO17 1BJ, U.K.

CORRESPONDING AUTHOR: M. WAGIH (e-mail: mahm1g15@ecs.soton.ac.uk)

This work was supported in part by the European Commission through the EnABLES Project through H2020-EU.1.4.1.2 under Grant 730957, and in part by the U.K. Engineering and Physical Sciences Research Council (EPSRC) under Grant EP/P010164/1.

Datasets from this article are available from the University of Southampton repository at <https://doi.org/10.5258/SOTON/D1632>.

This article has supplementary downloadable material available at <https://doi.org/10.1109/OJAP.2020.3038001>, provided by the authors.

**ABSTRACT** Additive manufacturing using direct-write or screen printing represent low-waste methods for fabricating antennas on low-cost flexible substrates. To realize rectennas using low-resolution printing methods, high-impedance antennas with simple printable geometries are required. This article proposes an electrically-small ( $0.212 \times 0.212 \lambda^2$ ) folded dipole antenna design with a scalable impedance for directly matching energy harvesting rectifiers. The antenna is demonstrated in a high-efficiency sub-1 GHz rectenna, with varying mesh fill-factors for optical transparency. The proposed solid (non-transparent) and meshed (70%-transparent) rectennas achieve a Power Conversion Efficiency (PCE) of over 70% and 60% from sub-1  $\mu\text{W}/\text{cm}^2$  power densities, at 940 and 920 MHz, respectively. This represents a 37% improvement in the PCE over state-of-the-art flexible rectennas while maintaining the smallest electrical size and simplest design by not requiring a matching network. The 70%-transparent rectenna's performance is investigated in real-life use-cases showing its suitability for ambient RF energy harvesting with over 500 mV DC output from a phone-call.

**INDEX TERMS** Antennas, dipole antennas, microstrip antennas, printed antennas, rectennas, rectifiers, RF energy harvesting, transparent antennas, wireless power transfer.

## I. INTRODUCTION

ADDITIVE manufacturing of antennas and passive Radio Frequency (RF) components has attracted significant interest. Low-cost planar antennas [1]–[11] as well as 3D-printed complex antenna structures [12]–[16] have been demonstrated using various low-cost additive manufacturing methods. The emerging high-density Internet of Things (IoT) market, with wearable and flexible electronics occupying a large sector [1], emphasizes the need for low-cost rapid fabrication processes, and printing-optimized antenna designs.

Direct-write dispenser printing is a thick-film deposition technique which has previously been used to realize electronic systems [17]. Dispenser printing has also been used to realize Ultra-high Frequency (UHF) antennas on flexible substrates such as polymers [11] and textiles [9]. Dispenser-printed antenna prototypes have shown similar performance (<3% discrepancy) to etched antennas of the same design

on the same substrate [11]. However, dispenser printing has only been used with standard antenna designs and no detailed investigation of printing-friendly antenna designs has been proposed. To explain, off-the-shelf low-cost dispenser printers have a low resolution (often around 0.3 mm), which may limit printing to antenna designs not requiring fine features, such as microstrip patch antennas [6]. Moreover, unlike subtractive manufacturing (e.g., etching or laser ablation), it is desirable to deposit less conductive ink to reduce the antenna's cost and fabrication time.

An example of antennas requiring small fine features are high-impedance co-designed antennas [18]. High-impedance, namely inductive, antennas have been used to match Metal-Oxide Semiconductor (MOS) devices, such as Radio Frequency Identification (RFID) ICs, or Schottky diodes, which have a highly-capacitive impedance. For example, rectennas which use co-designed antennas to directly match the rectifier's impedance have achieved a

higher Power Conversion Efficiency (PCE) than rectennas with stand-alone matching networks [18], [19]. However, recent electrically-small rectennas, [18], [20], [21], contain critical features under 0.5 mm which cannot be resolved using direct-write or screen printing. Another application of fine-featured small dipoles is UHF RFID [22], with dipole antennas incorporating built-in tuning loops becoming a standard for RFID antenna design [23].

Optically-transparent antennas have attracted significant interest recently for a range of applications such as smart displays [24], [25] and solar cell antennas [26]. Instead of relying on transparent conductive materials, transparent antennas can be realized using meshed non-transparent conductors (such as copper laminates) etched using traditional circuit fabrication techniques [24]. For example, a proximity-coupled patch antenna design was proposed based on meshed patches, [27], and demonstrated on a standard Rogers substrate. In addition, the effects of solar cell parameters on a microstrip patch were investigated using a meshed patch [28]. Furthermore, the impact of mesh fill-factors on a microstrip line's impedance, over a solid ground plane, were analyzed [29]. Nevertheless, there has been no investigation of a high-impedance antenna, typical for antenna-rectifier co-design [30] or RFID applications [23], based on a meshed geometry.

Unlike subtractive manufacturing techniques such as photolithography or milling of antennas out of solid metal, direct-write additive manufacturing techniques, such as inkjet, dispenser, and 3D printing directly benefit from meshed antennas. To explain, less ink is required to realize a meshed antenna compared to a solid design [31]. Thus, a lower mesh fill-factor not only enables optically-transparent antennas but also reduces the cost and manufacturing time of printed antennas.

This article presents a novel scalable high-impedance optically-transparent antenna fabricated using a low-cost off-the-shelf dispenser printer on a lossy substrate for energy harvesting applications. The novel contributions of this article can be summarized as:

- 1) A compact high-impedance dipole antenna design for additive manufacturing, eliminating features smaller than 1 mm. The antenna can be tuned parametrically to match RF Energy Harvesting (RFEH) rectifiers achieving State-of-the-Art (SoA) PCE while occupying an electrically-small area.
- 2) Investigating the performance of meshed rectennas based on the proposed dipole for applications requiring optical-transparency, and for reducing the printing cost and time by dispensing up to 70% less conductive material.

The solid and meshed rectennas maintain over 60% PCE from power densities as low as  $1 \mu\text{W}/\text{cm}^2$  for all mesh densities investigated (in Section V). The rectenna is then demonstrated in a real-life scenario (in Section VI) harvesting up to  $12.5 \mu\text{W}$  with 500 mV, across an 8 k $\Omega$  load, from the ambient emissions of a cellular phone.

This article presents the first investigation of a rectenna based on high-impedance meshed antennas for RFEH applications. Compared to state-of-the-art flexible rectennas, the proposed design achieves the highest PCE, with over 37% peak PCE-improvement over SoA for low power densities. The design maintains the smallest electrical size while having the lowest overall complexity due to not requiring a rectifier impedance matching or fine-featured antennas.

## II. ANTENNA FABRICATION BY DIRECT WRITING

Direct-write dispenser printing represents a hybrid material printing technique that combines the benefits of screen and inkjet printing [17]. Conductive ink, commonly a silver paste, is deposited directly on the substrate to form the conductive traces. Unlike screen printing and subtractive photolithography of copper sheets, dispenser printing is a zero-waste process. Only the required ink is deposited on the substrate and no conductive material is wasted.

With direct-write dispenser printing, it is possible to fabricate thicker conductive layers than with inkjet printing [2]. This reduces the surface resistivity, without printing additional layers or using a more expensive ink such as silver nano-wires (AgNW). It was previously shown that, with inkjet printing, three conductive layers may be needed to improve the radiation efficiency of a microstrip patch, which can reduce its mechanical reliability [5]. Furthermore, dispenser printing is more suitable for prototyping and low-volume manufacturing compared to photolithography and screen printing. Since no dark Ultra-Violet (UV) mask or printing screen are required, the up-front cost and the lead time can be minimized [11].

On the other hand, dispenser printing can have a lower throughput than screen printing and is less-suited to mass production. Nevertheless, being a thick-film technique, dispenser-printed antennas can be realized with screen printing. Compared to conventional PCBs, printing eliminates the need for photolithography equipment and photoresistive inks, and is compatible with a wider range of organic substrates. It was previously shown that by fabricating large-area systems on glass and other low-cost substrates, the material cost can reduce by up to 88%, compared to commercial RF laminates such as Rogers "low-cost" antenna-grade laminate [32].

The printer utilized in this article is a low-cost commercial Voltera V-One desktop printer, specified for prototyping circuit boards with minimal calibration of parameters such as the droplet size or the height of the dispensing nozzle. A silver ink of bulk resistivity  $9.5 \times 10^{-7} \Omega\text{m}$  is used. This translates to about 12 m $\Omega$ /square. However, at UHF bands, given the varying surface roughness of the ink, this can increase to 0.5  $\Omega$ /square. The fabrication steps shown in Fig. 1 are straightforward and can be summarized as:

- a) Planarizing the flexible substrate by adhering (using a spray or tape adhesive) it to a rigid surface.
- b) Dispensing the antenna's traces based on the CAD design.
- c) Thermal curing on a hot plate at 170°C for 40 minutes.

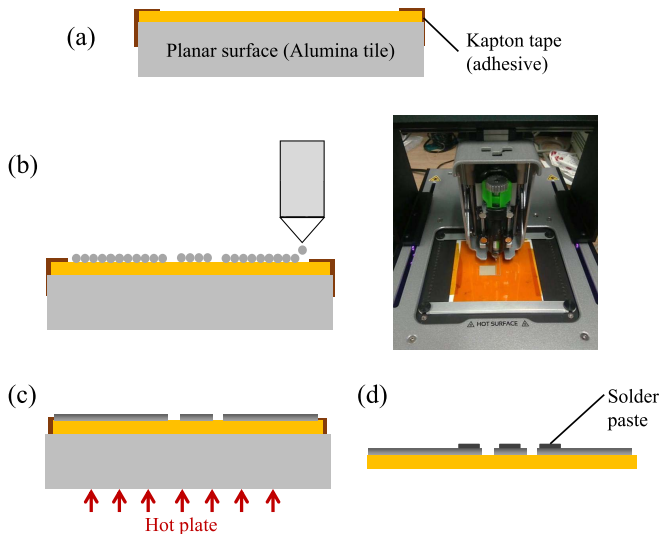


**FIGURE 1.** Flexible circuit fabrication steps using dispenser printing: (a) flexible substrate adhesion to a planar surface, (b) dispensing the conductive silver ink layer, (c) thermal curing of the ink, (d) mounting components and connectors using solder paste or low-temperature solder.

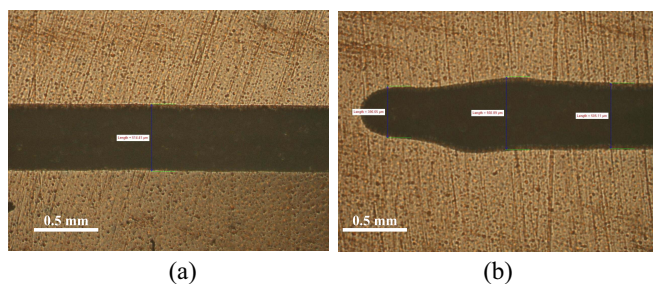


**FIGURE 2.** Micrograph of a 500  $\mu\text{m}$ -wide trace printed using dispenser printing: (a) trace edge, (b) continuous section of the trace.

d) Mounting the components using solder paste or low-temperature solder.

To evaluate the accuracy of dispenser printing and subsequently identify the minimum reproducible feature size, multiple conductive traces have been printed and examined. Fig. 2 shows micrographs of a dispenser-printed trace on a flexible Kapton substrate ( $\epsilon_r = 3.2$ ,  $\tan\delta = 0.02$ ) of 75  $\mu\text{m}$  thickness. It is observed that around 15  $\mu\text{m}$  non-uniformity can be observed on the edges of the printed line in Fig. 2-a. This represents an acceptable tolerance and will not affect the antenna's response. However, an open-ended trace (Fig. 2-b) may have variations in the width of up to 100  $\mu\text{m}$ . Thus, critical features of less than 0.5 mm need be avoided when designing the antenna, which reduces the fabrication tolerance to less than 5% and minimizes any impact on the antennas' impedance.

### III. ANTENNA DESIGN AND SIMULATION

#### A. HIGH IMPEDANCE ANTENNA DESIGN AND TUNING

A Folded-Dipole Antenna (FDA) can be designed with a high complex impedance allowing it to directly match capacitive loads such as MOS devices and Schottky

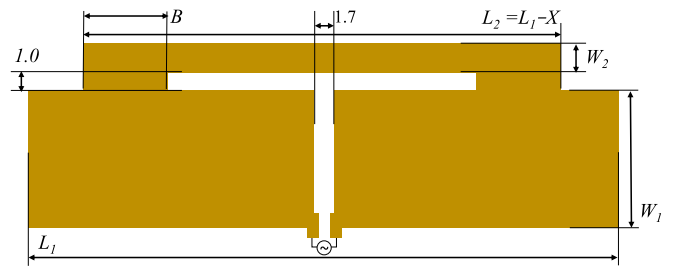


**FIGURE 3.** Layout and dimensions of the proposed high-impedance dispense printed FDA.

diodes. The designed antenna needs to be based on a predominantly-inductive FDA or a compact loop to achieve the desired highly-inductive input impedance. The antenna design proposed in [18], despite being parametrically-tunable, requires a fabrication process which can resolve features smaller than 200  $\mu\text{m}$ . Achieving such a high resolution using printed conductors would limit the antenna to high-resolution inkjet printing and certain conductive inks with droplet size less than 10  $\mu\text{m}$ . This would be impractical and require multiple layers to achieve a good thickness for the antenna to maintain high radiation efficiency [5], increasing both the antenna's cost and fabrication time. Therefore, for a tunable high-impedance FDA to be realized using commercial dispenser or screen printing, a novel design with a minimum feature size of at least 0.5 mm is needed. While the proposed antenna is realized using dispenser printing for rapid prototyping, the design is compatible with screen printing, which is more suited to mass production [6].

The proposed FDA geometry shown in Fig. 3 maintains a minimum feature size of 1 mm. Therefore, the antenna will be more resilient to fabrication imperfections such as non-uniform edges. The large dipole folds,  $W_1$  and  $W_2$ , along with the thick shorting terminals  $B$  are parametrically-tunable to achieve an input impedance matching that of a capacitive rectifier or an RFID IC. Additionally the ratio of  $L_1$  to  $L_2$ , controlled using  $X$  is used to control the resonant of the antenna and will therefore have the biggest influence on the real antenna impedance. Compared to a conventional dipole antenna, the proposed antenna contains a closed current return loop between the rectifier's terminals, eliminating the need for an additional shunt inductor [33]. In addition, the inductive slot enables simpler input impedance tuning to match rectifiers based on different diodes and for varying power levels.

The antenna has been simulated in CST Microwave Studio using a balanced feed to extract its input impedance. The conductivity of the model has been adjusted based on the measurements reported in the next section to improve the simulation accuracy. As the antenna is designed for sub-1 GHz RFEH and Wireless Power Transfer (WPT), the antenna needs to match the rectifier around 915 to 940 MHz, for it to be used for Industrial Scientific Medical (ISM)-band WPT as well as GSM 900 ambient RFEH. Parametric

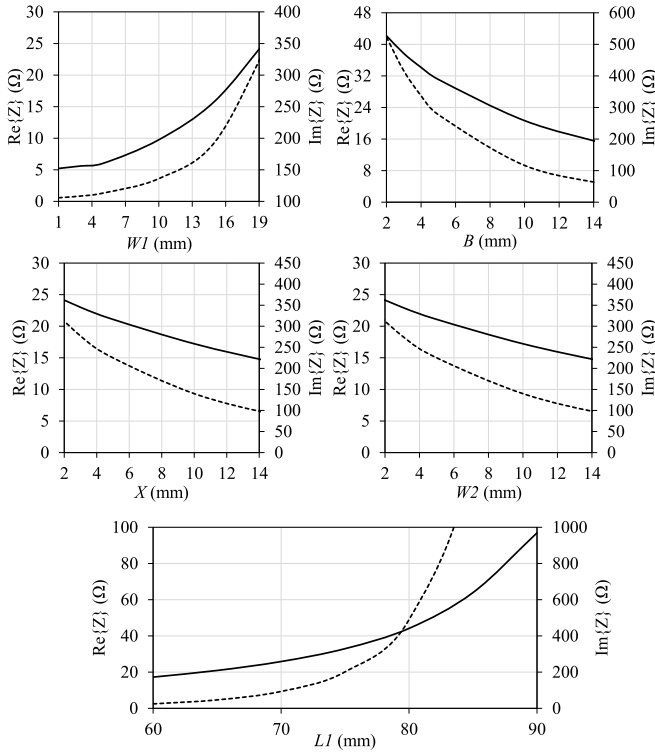


**FIGURE 4.** Real (dashed) and imaginary (solid) input impedance of the FDA as a function of the tuning parameters at 915 MHz; baseline parameters are  $L = 70$ ,  $X = 10$ ,  $B = 10$ ,  $W_1 = 15$ , and  $W_2 = 5$ .

studies of the antenna's impedance at 915 MHz have been performed to observe the variation based on scaling different antenna parameters. As explained in [18], increasing the width of the antenna's folds  $W_1$  or the shorting strip  $W_2$  would result in reducing the impedance of the antenna due to the increased fringing capacitance. Moreover the overall length of the antenna  $L_1$ , the length of the fold  $L_2$  and the shorting folds width  $B$  can be adjusted to control the resonance frequency of the antenna, which would in turn have the maximum impact on the impedance at any given frequency. Fig. 4 shows the antenna's input impedance at 915 MHz for variable  $L_1$ ,  $X$ ,  $B$ ,  $W_1$ , and  $W_2$ . The starting parameters, in mm, for each sweep are  $L_1 = 70$ ,  $X = 10$ ,  $B = 10$ ,  $W_1 = 15$ , and  $W_2 = 5$ . For the desired input impedance of  $Z_{\text{Antenna}} = 20 + j280\Omega$  at 930 MHz, the chosen parameter values (in mm) are  $L_1 = 58$ ,  $X = 2.5$ ,  $B = 10$ ,  $W_1 = 15$ , and  $W_2 = 5$ . Meshing of the proposed antenna is investigated in the next sub-section.  $Z_{\text{Antenna}}$  was selected based on the harmonic balance simulation of the rectifier, to maximize the PCE under  $-10$  dBm.

### B. MESHED ANTENNA DESIGN

As the antenna incorporates a large metal plane, this will increase the printing time and consume more ink, increasing the cost of the antenna. Furthermore, the antenna cannot be integrated in a transparent system such as solar cell-integrated antennas or display antennas [34]. Meshing the

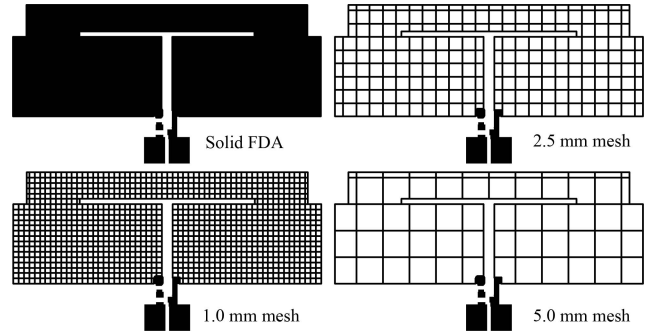


**FIGURE 5.** Layout of the FDA with different mesh spacing.

conductor, by perforating the antenna using variable fill-factors, can be introduced without significantly altering the antenna's performance. The mesh density or fill factor represents the ratio of the mesh lines to the grid-spacing. Fig. 5 shows the layout of the proposed solid antenna and for different mesh densities. The layout also shows the traces for a voltage doubler based on the SMS7630-079LF Schottky diode. The line width has been set to 0.3 mm, the smallest reproducible line using the Voltera V-One printer.

By reducing the mesh fill-factor, antennas of varying optical transparency can be realized. The optical transparency  $T_{\text{Mesh}}$  of a meshed antenna design is defined

$$T_{\text{Mesh}} = \left(1 - \frac{W_t}{W_t + W_G}\right)^2, \quad (1)$$

where  $W_t$  is the trace width and  $W_G$  is the size (length and width) of the gaps. This definition of an antenna's transparency is widely used and represents the ratio of metal-to-gaps [24]–[26], [29], [34], [35]. Therefore, the transparency of the antenna (mesh density) can also be regarded as the percentage of material reduction compared to a solid antenna. This is highly desirable for additive manufacturing to reduce the printing costs. After meshing, the printing time of the rectenna was reduced by over 80% to under 10 minutes for  $T_{\text{Mesh}} = 70\%$ , down from 55 minutes for the non-transparent antenna.

While the substrate used in this article is Kapton, which is only optically-translucent rather than transparent, various highly transparent variants of polyimide have been presented with similar dielectric properties to Kapton [36]. Kapton polyimide was used due to being commercially available widely from various vendors. In addition to transparent polyimide [36], other optically-transparent flexible substrates can be used without altering the antenna's response. For example, the PET substrate used for a microstrip antenna array in [37] has similar dielectric properties ( $\epsilon_r = 3.25$ ,  $\tan\delta = 0.02$  [37]) to the Kapton film used in this article. Thus, the proposed antenna's impedance and efficiency would not change if it was printed on PET. PDMS, a flexible but usually mm-thick substrate, has a  $\tan\delta = 0.021$  at 2.5 GHz [38]. Therefore, printing this antenna on PDMS will also not result in any performance degradation.

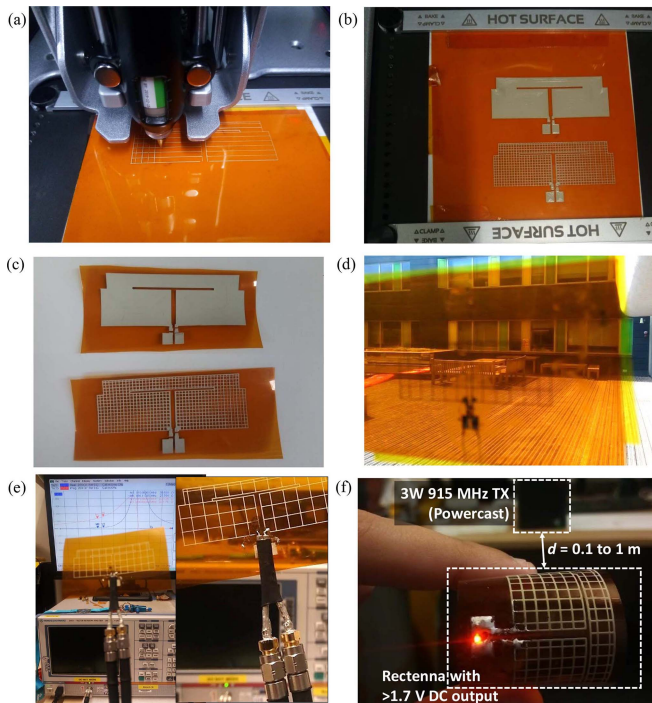


**FIGURE 6.** Dispenser-printed FDA prototypes photographs: (b) printed uncured ink on the polyimide substrate; (c) the cured solid and meshed FDAs; (d) demonstration of the assembled meshed rectenna's translucency; (e) differential impedance measurement with a coaxial jig and two-port VNA; (f) the assembled rectenna showing a  $>1.7$  V DC output lighting an LED.

The antenna prototypes are shown in Fig. 6 during (a) and after (b) printing, and after curing (c). In Fig. 6-d and e, the rectenna/antenna is shown with highly-translucent traces. Video 1 in the attached supplementary material shows the assembled rectenna in Fig. 6-f while producing over 1.7 V DC output required to light the LED at varying distances,  $0.1 < d < 1$  m, from a Powercast transmitter (3 W, 915 MHz) with various bending and crumpling radii.

### C. ANTENNA RADIATION PROPERTIES

The proposed antenna, being an electrically-small dipole, is expected to have omnidirectional radiation properties. The radiation patterns of the antenna were simulated in CST Microwave Studio. Fig. 7 shows the normalized simulated patterns over the azimuth and elevation planes. On both planes, the antenna achieves a high co/cross-polarization isolation. The peak directivity of the antenna is 1.85 dBi.

To investigate the impact of meshing on the antenna's performance, the gap width  $W_G$  was swept from 1 to 10 mm. It is expected that with a lower fill factor the antenna's (Ohmic) loss resistance will increase, which can reduce the radiation efficiency and gain. Fig. 8 shows the simulated radiation efficiency and gain as a function of  $W_G$ . Therefore, it is expected that antennas with a higher transparency will have a lower PCE.

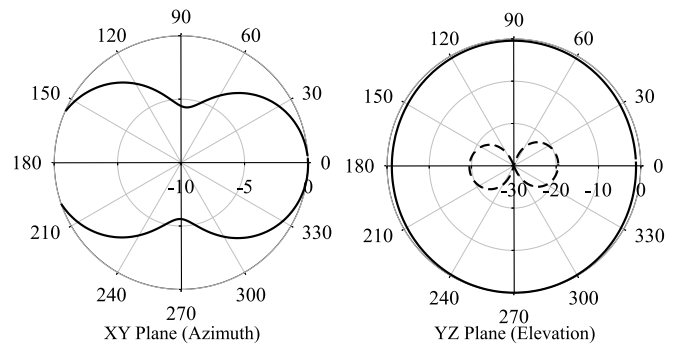


**FIGURE 7.** Normalized radiation patterns of the proposed antenna: co-polarized (solid) and cross-polarized (dashed).

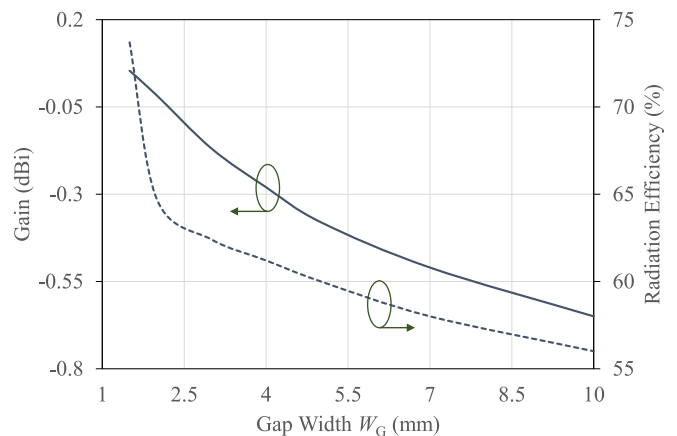


**FIGURE 8.** Simulated gain (solid) and radiation efficiency (dashed) of the antenna for varying  $W_G$ .

## IV. ANTENNA MEASUREMENTS

### A. SOLID ANTENNA MEASUREMENTS

A meshed FDA prototype, with 1 mm mesh spacing and 0.3 mm trace width has been fabricated to experimentally characterize its input impedance. The differential balanced-feed input impedance of the FDA has been measured using a two-port Vector Network Analyser (VNA) and a common-ground co-axial jig, using the method described in [39]. Fig. 6-e shows the balanced impedance measurement setup of the antenna. The feed point of the antenna resembles the position of the connection to the rectifier. Fig. 9 shows the simulated and measured impedance of the antenna up to 3 GHz. The frequency response of the fabricated antenna is observed to closely match the simulation model. However, around resonance, the fabricated antenna demonstrates lower imaginary and higher real impedance components compared to the simulation model. This indicates that the fabricated antenna has a lower quality factor compared to the simulation model due to additional resistive losses. The loss-discrepancy can be attributed to the conductivity utilized in the simulation model, and the surface roughness of the conductive ink, as the polyimide model utilized is material-accurate at the simulation frequency. Nevertheless, at the frequencies of

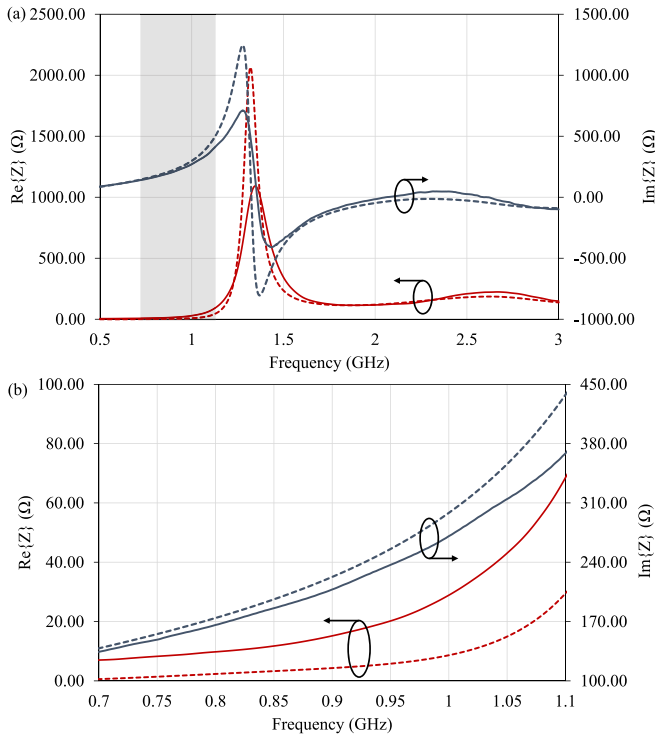


**FIGURE 9.** Simulated (dashed) and measured (solid) input impedance of the FDA with a 1 mm mesh spacing from 0.5 to 3 GHz (a) and around the 868/915 MHz ISM-bands (b).

interest, around 900 MHz, it is observed that the discrepancy in the imaginary impedance is less significant.

To achieve higher accuracy in the simulation model for optimizing the antenna, the surface resistance of the conductors in simulation has been varied to match the measured antenna impedance. The closest match between the simulation and measurements was obtained using a conductivity of  $2 \times 10^5 \sigma/m$  and a surface roughness of  $10 \mu m$ , this translates to about  $0.1 \Omega/square$  sheet resistance at 900 MHz.

### B. VARYING TRANSPARENCY INPUT IMPEDANCE MEASUREMENTS

The three meshed and the solid FDA have been fabricated to experimentally quantify the impact of the mesh density on the antenna's input impedance. Through this process, the mesh density could be utilized as an additional tuning parameter of the FDA's impedance.

The input impedance of the FDAs has been measured using the same balanced-feed coaxial jig. Fig. 10 shows the measured input impedance of the FDAs shown in Fig. 5. It is evident that the antenna's impedance is directly linked to the mesh density, where a lower mesh density results in higher input impedance. However, for up to 2.5 mm mesh-spacing, the variation in the reactance is less than 10% compared to the solid antenna. Therefore, the antennas with a mesh gap equal to or smaller than 2.5 mm are used in the rectenna evaluation without further tuning. The effect of a higher

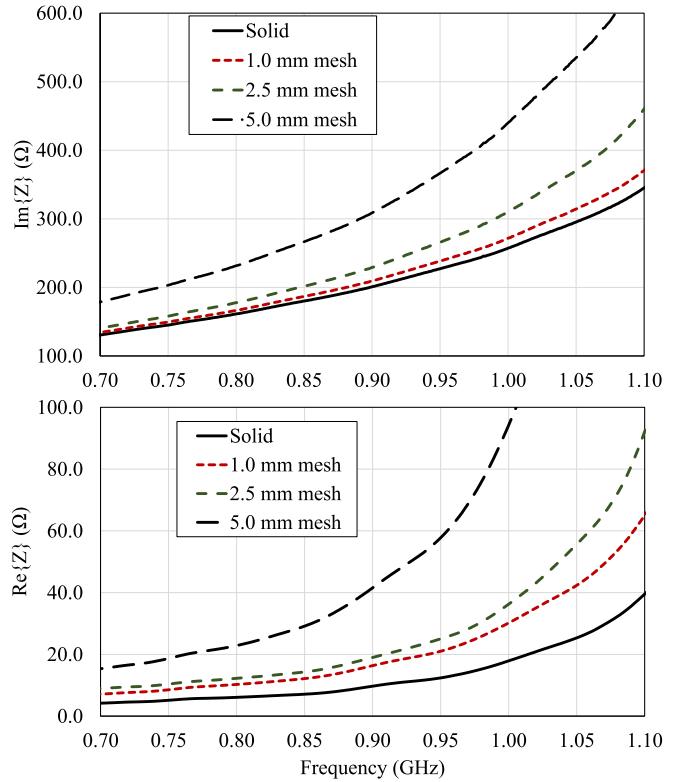


**FIGURE 10.** Measured real and imaginary input impedance of the proposed antenna based on varying mesh spacing for the same dimensions.

real input impedance on the rectifier's PCE is minimal, as discussed in the next section.

## V. RECTENNA MEASUREMENTS

### A. RECTIFIER DESIGN AND SIMULATIONS

A voltage doubler rectifier is selected for the printed rectenna implementation. In [19], it has been shown that a rectifier of predominantly reactive impedance can achieve higher PCEs. In addition, the UHF rectenna yielding the highest PCE using Schottky diodes in [18] has been designed based on antenna-rectifier co-design optimized at  $-20$  dBm RF power level based on a voltage doubler configuration.

The diode selected in this article is the Skyworks SMS7630. The rectifier can achieve high PCEs at sub-mW power levels owing to its very low measured forward voltage of 130 mV. The rectifier has been simulated using harmonic balance in Keysight ADS with the optimal input impedance  $Z_{rect}$ , optimized to achieve the lowest reflection coefficient below  $-10$  dBm [18]. An optimum input impedance of  $Z_{rect} = 20 + j280 \Omega$  has been extracted from harmonic balance simulation to achieve maximum PCE below  $-10$  dBm. While the rectifier's input impedance is expected to vary with frequency, optimizing the impedance at power levels below  $-15$  dBm results in maximizing the PCE for sub- $\mu W/cm^2$  power densities. The rectifier is tuned for 930 MHz to be able to harvest ambient RF power from GSM signals as well as Continuous Wave (CW) power at 915 MHz from a dedicated transmitter (e.g., Powercast/RFID reader).

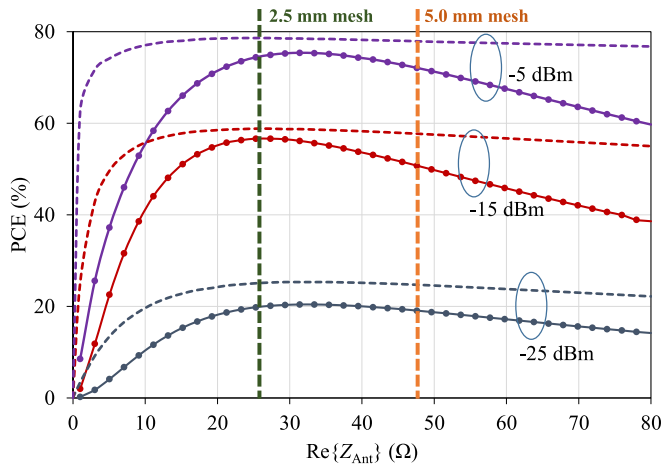


**FIGURE 11.** Simulated PCE of the rectifier including (solid) and excluding (dashed) mismatch, at 930 MHz with a 20 kΩ load, for varying  $\Re\{Z_{Ant}\}$ .

Fig. 11 shows the rectifier’s simulated PCE at 930 MHz for varying real antenna impedances, at different RF power levels. The solid lines represent the PCE calculated as  $P_{DC}/P_{RF}$ , inclusive of impedance mismatch losses. On the other hand, the dashed lines represent the maximum achievable PCE exclusive of mismatch, calculated as  $P_{DC}/P_{accepted}$ . As observed in Fig. 10, the real impedance of the antenna can vary significantly based on the mesh fill-factor (i.e., the transparency). Therefore, the rectifier’s PCE has been simulated as a function of  $\Re\{Z_{Ant}\}$ . In Fig. 11, it can be seen that for up to 5 mm  $W_G$ , the PCE, inclusive of impedance mismatch, stays within 10% of the peak PCE of the rectifier.

### B. RECTENNA DC MEASUREMENTS

To characterize the rectennas’ DC output and PCE, a 10 dBi directional antenna with a CW input are used to wirelessly-power the rectenna with varying power densities  $S$ . The rectenna is placed at 1.1 m from the source, which satisfies the minimum Fraunhofer far-field distance of 0.88 m based on the transmitting antenna’s length of 40 cm. Fig. 12 shows the schematic and photograph of the rectennas’ test setup.

The power density  $S$  at the antenna was calculated based on the electric field  $E$  given by

$$E = \frac{\sqrt{30P_T G_T}}{d} \quad (2)$$

$$S = \frac{E^2}{120\pi} \quad (3)$$

where  $P_T$  and  $G_T$  are transmitted power and gain, respectively, and  $d$  being the transmitter-rectenna separation. The received power is subsequently calculated based on the antenna’s effective area given by

$$A_{eff} = G_R \frac{\lambda^2}{4\pi} \quad (4)$$

where  $G_R$  is the rectenna’s gain obtained from the CST simulation.  $A_{eff}$  of the non-transparent, 50%-transparent

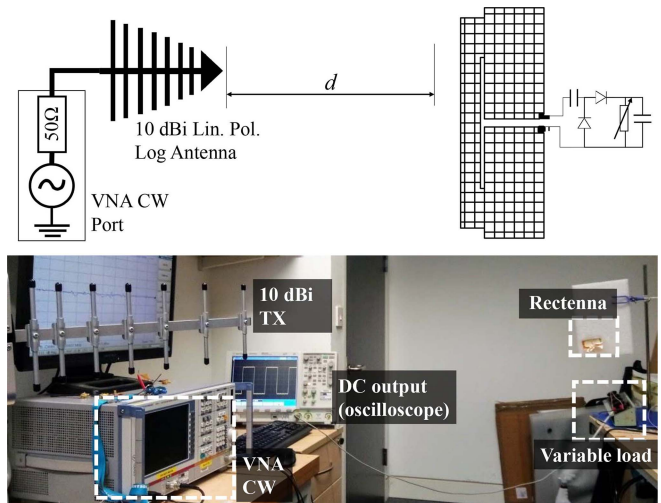


**FIGURE 12.** Wireless measurement setup of the meshed high-impedance rectenna using a directional transmitter.

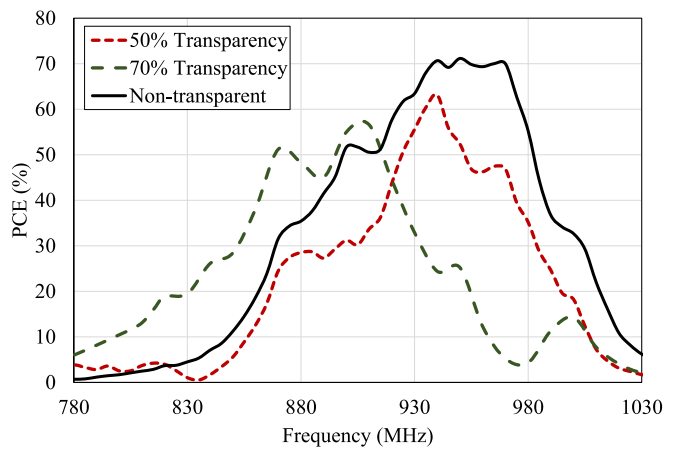


**FIGURE 13.** Measured PCE of the proposed non transparent, 50% and 77% transparent rectennas from  $S = 0.88 \mu\text{W}/\text{cm}^2$  for a 7 kΩ load at variable frequencies.

and 70%-transparent rectennas were calculated using a peak directivity of 1.6, 1.4, and 1.0 (linear dimensionless), respectively. The PCE is then calculated using

$$PCE = \frac{V^2}{Z_L} \times \frac{1}{P_{RX}} \quad (5)$$

where  $V$  is the DC voltage across a load of  $Z_L$  impedance. This setup has been widely used to evaluate rectennas [40]–[42], and includes the rectification as well as impedance mismatch losses. By using the antenna’s lossless directivity as  $G_T$ , the antenna losses are factored in the PCE which enables holistic evaluation of the rectenna. This prevents overestimation of the PCE due to any inaccuracies in the gain or radiation efficiency figures obtained from the CST antenna simulations, due to variations in the material properties.

A frequency sweep was carried out for a fixed transmitted power (12 dBm–0.5 dB cable loss) corresponding to  $0.88 \mu\text{W}/\text{cm}^2$ . Fig. 13 shows the rectennas’ PCE across the

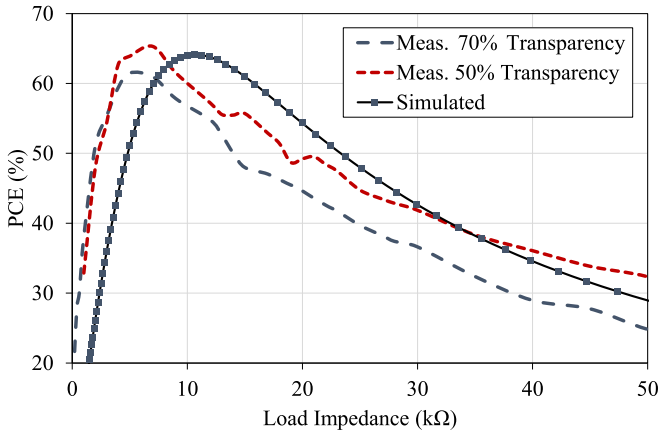


**FIGURE 14.** Simulated rectifier PCE for a varying load and rectenna measurements for 77% and 50%-transparency from  $S = 1 \mu\text{W}/\text{cm}^2$ .

sub-1 GHz license free 868/915 MHz and GSM900 bands. It can be seen that with increasing transparency the rectennas' resonance shifts to a lower frequency. This is attributed to the increasing  $\Re\{Z_{Ant}\}$  and  $\Im\{Z_{Ant}\}$  with reducing fill-factor previously measured in Fig. 10. The results in Fig. 13 were measured across a  $7 \text{ k}\Omega$  load.

A resistive load sweep was carried out to identify the maximum power transfer point of the rectennas. Fig. 14 shows the simulated and measured PCE as a function of the load impedance. It is observed that the antennas' varying transparency does not affect the optimal load despite having different  $\Re\{Z_{Ant}\}$ . The rectennas' optimal measured load of  $7 \text{ k}\Omega$  is suitable for integration with commercial and custom boost converters such as [42] and [43], respectively.

Three rectennas were characterized under varying  $S$ : a non-transparent solid rectenna, a 70%-transparent (2.5 mm mesh-spacing) rectenna, and a 50%-transparent (1 mm mesh-spacing) rectenna. To demonstrate the rectenna's high PCE at low power levels, the CW input was varied from  $-11$  to  $15.5 \text{ dBm}$ , to present the rectenna with  $0.005 < S < 2 \mu\text{W}/\text{cm}^2$ . Fig. 15 and 16 show the PCE and the DC voltage output of the rectennas.

As observed in Fig. 15, the solid rectenna has an improved PCE and sensitivity, achieving  $\text{PCE} = 50\%$  at approximately 50% lower power than its transparent counterpart. The PCE of the 70%-transparent rectenna reaches 60% for  $S = 0.66 \mu\text{W}/\text{cm}^2$ . Additionally, the DC voltage output of all three prototypes of varying transparency exceeds  $325 \text{ mV}$  from  $S = 0.25 \mu\text{W}/\text{cm}^2$ . This represents over  $2\times$  sensitivity improvement over SoA compact rectennas designed for ultra-low power transmission [42], where a minimum of  $S = 0.62 \mu\text{W}/\text{cm}^2$  was required to achieve the  $330 \text{ mV}$  required for starting-up a commercial DC-DC boost converter.

### C. RECTENNA RADIATION EFFICIENCY CALCULATION

From the calculated PCE in Fig. 15, it is possible to estimate the antennas' radiation efficiency. At  $-15 \text{ dBm}$ , the

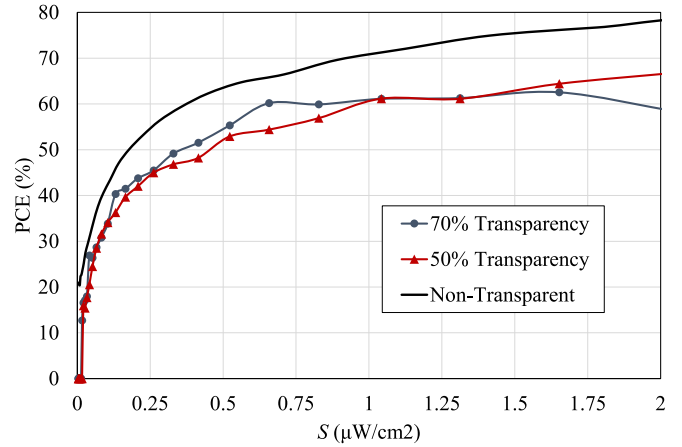


**FIGURE 15.** Measured PCE of the proposed non transparent, 50% and 70% transparent rectennas from an incident plane wave  $S$ , for a  $7 \text{ k}\Omega$  load.

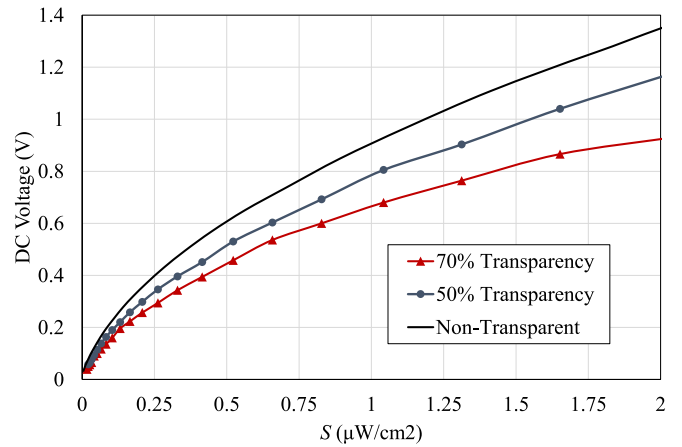


**FIGURE 16.** Measured DC voltage of the non-transparent, 50%, and 70%-transparent rectennas from an incident plane wave  $S$ , across a  $7 \text{ k}\Omega$  load.

rectifier has a simulated PCE of 57% with the optimum source impedance of  $20 + j280 \Omega$ . Using the non-transparent antenna's simulated directivity of 1.6,  $-15 \text{ dBm}$  can be received from a power density  $S = 0.18 \mu\text{W}/\text{cm}^2$ . At  $S = 0.18 \mu\text{W}/\text{cm}^2$ , the proposed rectennas achieve 50%, 42%, and 43%, PCE, for 0%, 50% and 70% transparency, respectively. Therefore, the radiation efficiency of the antennas can be estimated, relative to the PCE achievable by a loss-less source. The calculated radiation efficiency is 88%, 74%, 75% for the non-transparent, 50%-transparent and 70%-transparent antennas.

The drop in the radiation efficiency between the non-transparent and transparent rectennas correlates with the simulated results in Fig. 8, and with the previously reported observations in [26]. Between the 50%- and 70%-transparent rectennas, the variation in the calculated radiation efficiency could be attributed to fabrication tolerances and uncertainties in the test setup, resulting in minimal impact of the antenna's transparency on its effective PCE. It was previously noted

**TABLE 1.** Comparison of the proposed rectenna with flexible, transparent and printed harvesters.

| Study        | Conductor                                   | Substrate                                               | Optical transparency | Frequency (GHz) | Peak PCE at $S$                    | PCE at $S=0.5$ $\mu\text{W}/\text{cm}^2$ (%) | DC V at $S=1$ $\mu\text{W}/\text{cm}^2$ | Electrical size ( $\lambda_0^3$ )        | Complexity       |
|--------------|---------------------------------------------|---------------------------------------------------------|----------------------|-----------------|------------------------------------|----------------------------------------------|-----------------------------------------|------------------------------------------|------------------|
| This work    | Silver ink, $2 \times 10^5 \sigma/\text{m}$ | Kapton, $\tan\delta=0.02$                               | NTA                  | 0.94            | 78.5% at $S=2$                     | 64.8%                                        | 0.9                                     | $0.212 \times 0.212 \times 0.0003$       | Very simple (2D) |
| This work    | Silver ink, $2 \times 10^5 \sigma/\text{m}$ | Kapton, $\tan\delta=0.02$                               | 70%                  | 0.92            | 62.5% at $S=1.7$                   | 55%                                          | 0.65                                    | $0.212 \times 0.212 \times 0.0003$       | Very simple (2D) |
| TAP'13 [45]  | Conductive fabric                           | pile+jeans, $\tan\delta_1=0.009$ , $\tan\delta_2=0.023$ | NTA                  | 0.876           | 50%                                | NR                                           | NR, $<0.5$ V*                           | $0.702 \times 0.556 \times 0.0088$       | Simple (2D)      |
| TMTT'18 [42] | Copper taper                                | paper ( $\tan\delta=0.05$ )                             | NTA                  | 0.9             | 57% at $S=6$                       | 36% $\ddagger$                               | 0.25 $\ddagger$                         | $0.337 \times 0.337 \times 0.028$        | Simple (2D)      |
| TMTT'19 [26] | $\mu$ mesh conductor                        | Glass + RO5880                                          | 92.4%                | 2.45            | $\approx 49\%$ $\ddagger$ at $S=5$ | 45% $\ddagger$                               | 1.5 $\ddagger$                          | $1.23 \times 1.23 \times 0.3^{\ddagger}$ | Complex (3D)     |
| TAP'20 [7]   | Silver ink                                  | LCP                                                     | NTA                  | 2.45            | 40% at 0 dBm                       | NR                                           | NR                                      | $0.37 \times 0.205 \times 0.0015$        | Simple (2D)      |
| TAP'20 [41]  | Conductive fabric                           | Felt, $\tan\delta=0.02$                                 | NTA                  | 0.83            | 53%                                | 53%                                          | 0.67                                    | $0.33 \times 0.33 \times 0.003$          | Simple (2D)      |

NTA: non-transparent antenna;  $\ddagger$  thickness estimated from photograph based on length of SMA joints; \*estimated from the output at  $S=3 \mu\text{W}/\text{cm}^2$ ;  $\ddagger$  estimated from the graphs

that wireless testing of rectennas can incur  $\pm 1$  dB error in the incident power [43].

#### D. COMPARISON WITH PREVIOUS WORK

The proposed rectenna is compared, in Table 1, to SoA printed, flexible, or textile-based RF energy harvesters, as well as a complex 3D transparent rectenna. It can be observed that despite the overall low complexity of the design, and its implementation using silver inks with relatively low conductivity on lossy ( $\tan\delta = 0.02$ ) substrate, the proposed rectenna achieves the highest PCE for  $S < 1 \mu\text{W}/\text{cm}^2$ , compared to rectennas operating at similar frequencies such as [40], [41], [44], owing to the precise antenna co-design with the rectifier achieving minimal reflection and a high voltage input at the rectifier's terminal. It can also be seen that despite being electrically smaller than other implementations (at similar and higher frequencies), the proposed rectenna achieves a surpassing DC voltage showing improved RFEH performance. Finally, the proposed rectenna is the only transparent 2D rectenna built entirely using low-cost materials on a flexible substrate while maintaining a high PCE from sub- $\mu\text{W}/\text{cm}^2$  power densities.

Compared to the high-efficiency textile rectenna in [40], the proposed rectenna achieves over 20% higher peak PCE, at the same  $S$ , due to the improved impedance matching and avoiding lumped components. While [26] achieves a very high DC voltage from ultra-low power densities, this is only achieved when the output of eight antenna elements, each having an individual rectifier, is combined; the output from a single port does not exceed 0.5 V for  $S$  as high as  $5.5 \mu\text{W}/\text{cm}^2$ . In addition, the size of the proposed rectenna is more compact, when compared to

the wavelength, than the individual patch elements in [26]. This would result in a higher DC output from a large-area rectenna array implementation based on the proposed antenna.

The complexity of the proposed rectenna is the lowest compared to other rectennas in Table 1 due to:

- 1) the ability to be directly printed on any conformable thin and light substrate;
- 2) not utilizing a standalone matching network;
- 3) having the smallest electrical size (area and volume) with the ability to be meshed for optical transparency and material-reduction.

Other conformable rectennas on low-cost substrates (textiles and paper) such as [40], [41], [44] utilize lumped components, namely inductors, for impedance matching. Such inductors not only occupy additional space but also significantly increase the cost of the rectenna in mass production, compared to passive low-cost printed antenna traces. Finally, the proposed rectenna (70%-transparent and non-transparent) achieves the highest PCE compared to the rectennas in Table 1, showing its suitability for low power RFEH applications. In the next section, the proposed antenna is demonstrated in a practical RFEH use-case.

#### VI. INDOOR UP-LINK AMBIENT ENERGY HARVESTING

Ambient RFEH from cellular networks has been investigated [45]–[48]. In multiple reported wireless Power Spectral Density (PSD) surveys, the GSM 900 band consistently had the highest available power [45], [47], [49]. RFEH from the up-link (i.e., from a phone) has previously been investigated showing up to  $17\times$  higher mean RF PSD in busy indoor environments, such as a train,

compared to down-link [48]. By observing the transient DC output of the rectenna in time-domain, for a variety of real cellular emissions, it is possible to assess the validity of RFEH from the up-link. In addition, by calculating the transient harvested DC power, it is possible to predict and model the behavior of low-power intermittent systems such as [50], when powered using rectennas.

The proposed rectenna, with a 70% transparency, was used to harvest the ambient radiation from a smartphone in an office environment. The down-link PSD was measured, using a spectrum analyzer and a simple dipole, to be under  $-40$  dBm in the room where the test was carried. Hence, in this environment, the down-link RF power level is too low to be harvested using any of the rectifiers reported in literature [51]. The phone was placed at 7 cm from the rectenna adhered to a wooden desk demonstrating a potential use-case in an office. The DC output of the rectenna was measured using an oscilloscope ( $\times 10$  probe) across a  $20\text{ k}\Omega$  load. The inset in Fig. 17-a shows the indoor ambient RFEH test setup; the supplementary videos show the DC voltage measurements for the traces in Fig. 17.

The measured DC output of the rectenna was recorded for various phone activities. First of all, the DC output was measured when the phone was idle, before and after receiving a text message (SMS), shown in Fig. 17-a. The peak DC power generated from the idle phone is  $1.2\ \mu\text{W}$  with 155 mV. While such output can supply a commercial power management circuit such as the Analog ADP5090 (minimum operational voltage = 80 mV) with sufficient DC voltage and current, the output is highly varying and comes in  $<50$  ms bursts. However, when the idle phone is receiving an SMS, the DC power harvested peaks at  $3.8\ \mu\text{W}$  with  $>250$  mV over a longer stable 4 s period. This represents a  $15\ \mu\text{J}$  DC energy yield which can enable intermittent computation on a commercial low-power micro-controller, while the power is being generated [50].

The second case considered is voice-calls. Before the phone rings the “idle” DC power harvested increases to  $4.5\ \mu\text{W}$  (300 mV), in 30 ms periods. While the phone is ringing, the DC output stabilizes at  $12.5\ \mu\text{W}$  (500 mV) for the entire duration, as shown in Fig. 17-b. To demonstrate the variations that could arise from movements of the phone, the phone was moved in the  $20\times 20\times 15$  cm space surrounding the rectenna. The phone was also rotated by  $90^\circ$  while moving to demonstrate potential polarization misalignment between the phone and the rectenna. Fig. 17-b, from 16 s, shows the effects of moving the phone on the DC output. The sharp drop observed around 17 s is caused by the phone’s linear polarization being cross-polarized with respect to the rectenna, resulting in a very low polarized gain. When aligned, it is shown that the variations in distance can reduce the DC voltage by around 50%. The incoming call is declined at 49 s showing a drop in the DC output to  $<20$  mV. Video 2 in the supplementary multi-media file shows the movement of the phone while measuring the output in

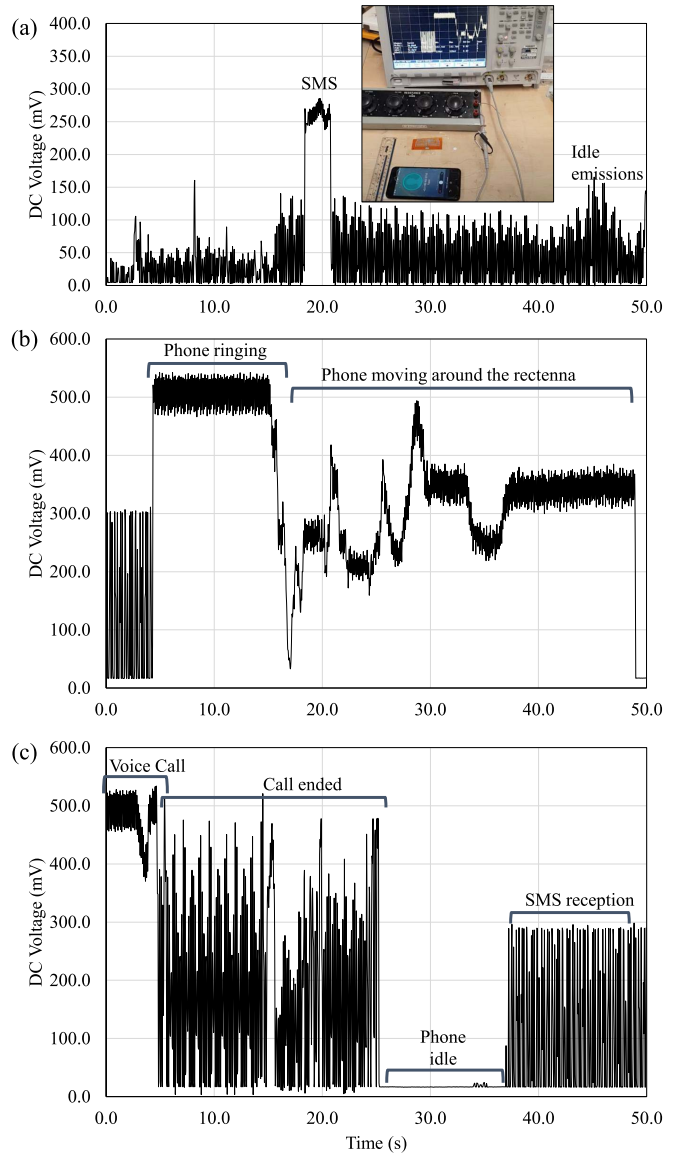


**FIGURE 17.** The rectenna’s DC output when harvesting ambient RF power from a GSM-connected phone: (a) idle phone emissions and short message reception, inset shows the measurement setup; (b) voice call while moving the phone around the rectenna; (c) end of a voice call.

Fig. 17-b. The same process is repeated for a voice-call which is accepted. It can be seen in Fig. 17-c that as soon as the call is accepted, at 4.5 s, the stable RF transmission is interrupted and the harvested voltage shows up in 30 ms bursts instead.

A previous demonstration of a flexible rectenna harvesting from a ringing phone at GSM frequency was reported in [41]. The output of the paper rectenna in [41] (previously compared in Table 1), when put in contact ( $<1$  cm clearance) with the phone, was 360 mV. The proposed rectenna on the other hand has a 500 mV output at over 7 cm from the phone, and 300-500 mV DC output with the phone moving up to 20 cm away from the rectenna. This is due to the improved voltage sensitivity at lower power levels, as well

as improved PCE, as characterized with a power-calibrated CW source in the previous section.

## VII. CONCLUSION

In this article, a direct-write high impedance printed antenna is proposed for energy harvesting applications. The antenna's geometry, designed with  $>1$  mm features to accommodate all low-cost printing processes, can be tuned to match high-impedance capacitive rectifiers. The proposed antenna has been meshed using various fill factors to demonstrate the feasibility of optically-transparent RFEH without matching networks. The rectenna achieves a SoA PCE of 70% and 60%, for the non-transparent and 70%-transparent rectennas, respectively, for power densities below  $1 \mu\text{W}/\text{cm}^2$ . A 1 V DC output is achieved by the non-transparent and 50%-transparent rectennas from  $1.5 \mu\text{W}/\text{cm}^2$  with an optimal input impedance less than  $7 \text{ k}\Omega$ , in line with commercial and SoA boost converters. The rectenna has been demonstrated for ambient RFEH with a  $12.5 \mu\text{W}$  DC output with 500 mV harvested from a phone call. It is concluded that meshed rectennas are suitable for RFEH applications with less than 14% lower PCE compared to their solid counterparts despite using up to 70% less conductive material and maintaining a high optical transparency.

## REFERENCES

- [1] S. A. Nauroze *et al.*, "Additively manufactured RF components and modules: Toward empowering the birth of cost-efficient dense and ubiquitous IoT implementations," *Proc. IEEE*, vol. 105, no. 4, pp. 702–722, Apr. 2017.
- [2] B. S. Cook and A. Shamim, "Inkjet printing of novel wideband and high gain antennas on low-cost paper substrate," *IEEE Trans. Antennas Propag.*, vol. 60, no. 9, pp. 4148–4156, Sep. 2012.
- [3] M. Wagih, A. S. Weddell, and S. Beeby, "Millimeter-wave power harvesting: A review," *IEEE Open J. Antennas Propag.*, vol. 1, pp. 560–578, 2020.
- [4] B. S. Cook, B. Tehrani, J. R. Cooper, and M. M. Tentzeris, "Multilayer inkjet printing of millimeter-wave proximity-fed patch arrays on flexible substrates," *IEEE Antennas Wireless Propag. Lett.*, vol. 12, pp. 1351–1354, 2013.
- [5] W. G. Whittow *et al.*, "Inkjet-printed microstrip patch antennas realized on textile for wearable applications," *IEEE Antennas Wireless Propag. Lett.*, vol. 13, pp. 71–74, 2014.
- [6] A. Meredov, K. Klionovski, and A. Shamim, "Screen-printed, flexible, parasitic beam-switching millimeter-wave antenna array for wearable applications," *IEEE Open J. Antennas Propag.*, vol. 1, pp. 2–10, 2019.
- [7] A. Eid, J. Hester, J. Costantine, Y. Tawk, A. H. Ramadan, and M. M. Tentzeris, "A compact source-load agnostic flexible rectenna topology for IoT devices," *IEEE Trans. Antennas Propag.*, vol. 68, no. 4, pp. 2621–2629, Apr. 2020.
- [8] Z. Ali *et al.*, "Authentication using metallic inkjet-printed chipless RFID tags," *IEEE Trans. Antennas Propag.*, vol. 68, no. 5, pp. 4137–4142, May 2020.
- [9] Y. Li, R. Torah, S. Beeby, and J. Tudor, "Fully direct-write dispenser printed dipole antenna on woven polyester cotton fabric for wearable electronics applications," *Electron. Lett.*, vol. 51, no. 17, pp. 1306–1308, Aug. 2015.
- [10] S. F. Jilani, M. O. Munoz, Q. H. Abbasi, and A. Alomainy, "Millimeter-wave liquid crystal polymer based conformal antenna array for 5G applications," *IEEE Antennas Wireless Propag. Lett.*, vol. 18, no. 1, pp. 84–88, Jan. 2019.
- [11] M. Wagih, "Direct-write dispenser printing for rapid antenna prototyping on thin flexible substrates," in *Proc. Eur. Conf. Antennas Propag. (EuCAP)*, 2020, pp. 1–4.
- [12] J. Kimionis, M. Isakov, B. S. Koh, A. Georgiadis, and M. M. Tentzeris, "3D-printed origami packaging with inkjet-printed antennas for RF harvesting sensors," *IEEE Trans. Microw. Theory Techn.*, vol. 63, no. 12, pp. 4521–4532, Dec. 2015.
- [13] G. McKerricher, D. Titterington, and A. Shamim, "A fully inkjet-printed 3-D honeycomb-inspired patch antenna," *IEEE Antennas Wireless Propag. Lett.*, vol. 15, pp. 544–547, 2015.
- [14] S. Wang, L. Zhu, and W. Wu, "3-D printed inhomogeneous substrate and superstrate for application in dual-band and dual-CP stacked patch antenna," *IEEE Trans. Antennas Propag.*, vol. 66, no. 5, pp. 2236–2244, May 2018.
- [15] Z.-X. Xia, K. W. Leung, and K. Lu, "3-D-printed wideband multi-ring dielectric resonator antenna," *IEEE Antennas Wireless Propag. Lett.*, vol. 18, pp. 2110–2114, 2019.
- [16] K. Johnson *et al.*, "Digital manufacturing of pathologically-complex 3D printed antennas," *IEEE Access*, vol. 7, pp. 39378–39389, 2019.
- [17] Y. Zheng, Z. He, Y. Gao, and J. Liu, "Direct desktop printed-circuits-on-paper flexible electronics," *Sci. Rep.*, vol. 3, p. 1786, May 2013.
- [18] M. Wagih, A. S. Weddell, and S. Beeby, "High-efficiency sub-1 GHz flexible compact rectenna based on parametric antenna-rectifier co-design," in *Proc. IEEE MTT-S Int. Microw. Symp.*, 2020, pp. 1066–1069.
- [19] H. J. Visser, S. Keyrouz, and A. B. Smolders, "Optimized rectenna design," *Wireless Power Transf.*, vol. 2, no. 1, pp. 44–50, 2017.
- [20] W. Lin and R. W. Ziolkowski, "Electrically small huygens CP rectenna with a driven loop element maximizes its wireless power transfer efficiency," *IEEE Trans. Antennas Propag.*, vol. 68, no. 11, pp. 540–545, Jan. 2020.
- [21] W. Lin and R. W. Ziolkowski, "Electrically small, single-substrate huygens dipole rectenna for ultra-compact wireless power transfer applications," *IEEE Trans. Antennas Propag.*, early access, Jul. 1, 2020, doi: [10.1109/TAP.2020.3004987](https://doi.org/10.1109/TAP.2020.3004987).
- [22] M. Wagih, Y. Wei, A. Komolafe, R. Torah, and S. Beeby, "Reliable UHF long-range textile-integrated RFID tag based on a compact flexible antenna filament," *Sensors*, vol. 20, no. 12, p. 3435, 2020.
- [23] G. Marrocco, "The art of UHF RFID antenna design: Impedance-matching and size-reduction techniques," *IEEE Antennas Propag. Mag.*, vol. 50, no. 1, pp. 66–79, Feb. 2008.
- [24] Z. J. Silva, C. R. Valenta, and G. Durgin, "Optically transparent antennas: A survey of transparent microwave conductor performance and applications," *IEEE Antennas Propag. Mag.*, early access, May 18, 2020, doi: [10.1109/MAP.2020.2988526](https://doi.org/10.1109/MAP.2020.2988526).
- [25] P. D. Tung and C. W. Jung, "Optically transparent wideband dipole and patch external antennas using metal mesh for UHD TV applications," *IEEE Trans. Antennas Propag.*, vol. 68, no. 3, pp. 1907–1917, Mar. 2020.
- [26] Y. Zhang, S. Shen, C. Y. Chiu, and R. Murch, "Hybrid RF-solar energy harvesting systems utilizing transparent multiport micromeshed antennas," *IEEE Trans. Microw. Theory Techn.*, vol. 67, no. 11, pp. 4534–4546, Nov. 2019.
- [27] T. Yasin and R. Baktur, "Bandwidth enhancement of meshed patch antennas through proximity coupling," *IEEE Antennas Wireless Propag. Lett.*, vol. 16, pp. 2501–2504, 2017.
- [28] T. Yekan and R. Baktur, "Communication study of the impact between a triple junction space solar cell and the antenna integrated on top of it," *IEEE Trans. Antennas Propag.*, early access, Aug. 20, 2020, doi: [10.1109/TAP.2020.3016864](https://doi.org/10.1109/TAP.2020.3016864).
- [29] Z. J. Silva, C. R. Valenta, and G. D. Durgin, "Design and characterization of meshed microstrip transmission lines," in *Proc. IEEE Int. Microw. Symp.*, Boston, MA, USA, 2019, pp. 811–814.
- [30] M. Wagih, A. S. Weddell, and S. Beeby, "Rectennas for radio-frequency energy harvesting and wireless power transfer: A review of antenna design [antenna applications corner]," *IEEE Antennas Propag. Mag.*, vol. 62, no. 5, pp. 95–107, Oct. 2020.
- [31] R. Martinez *et al.*, "Circularly polarized shorted ring slot rectenna with a mesh design for optimized inkjet printing on paper substrate," in *Proc. 9th Eur. Conf. Antennas Propag. (EuCAP)*, Lisbon, Portugal, 2015, pp. 1–3.
- [32] E. Shi, E. Centeno, R. Figueroa, C. Qi, and G. Durgin, "A rectenna using copper foil on glass to reduce cost of space solar power," in *Proc. IEEE Wireless Power Transf. Conf. (WPTC)*, London, U.K., 2019, pp. 421–425.

- [33] C. Domnik, S. Husges, and C. Degen, "Frugal energy harvesting: Microwave energy radiated into the environment from wireless networks," *IEEE Microw. Mag.*, vol. 21, no. 1, pp. 82–87, Jan. 2020.
- [34] Z. J. Silva, C. P. Hunter, C. R. Valenta, and G. D. Durgin, "2.5 GHz meshed inset-fed patch antenna," in *Proc. IEEE Int. Symp. Antennas Propag. USNC-URSI Radio Sci. Meeting*, 2019, pp. 843–844.
- [35] R. Yazdani, M. Yousefi, H. Aliakbarian, H. Oraizi, and G. A. E. Vandenbosch, "Miniaturized triple-band highly transparent antenna," *IEEE Trans. Antennas Propag.*, vol. 68, no. 2, pp. 712–718, Feb. 2020.
- [36] H.-J. Ni, J.-G. Liu, Z.-H. Wang, and S.-Y. Yang, "A review on colorless and optically transparent polyimide films: Chemistry, process and engineering applications," *J. Ind. Eng. Chem.*, vol. 28, no. 25, pp. 16–27, 2015.
- [37] A. T. Castro and S. K. Sharma, "Inkjet-printed wideband circularly polarized microstrip patch array antenna on a PET film flexible substrate material," *IEEE Antennas Wireless Propag. Lett.*, vol. 17, pp. 176–179, 2018.
- [38] A. S. M. Sayem, R. B. V. B. Simorangkir, K. P. Esselle, and R. M. Hashmi, "Development of robust transparent conformal antennas based on conductive mesh-polymer composite for unobtrusive wearable applications," *IEEE Trans. Antennas Propag.*, vol. 67, no. 12, pp. 7216–7224, Dec. 2019.
- [39] K. Palmer and M. van Rooyen, "Simple broadband measurements of balanced loads using a network analyzer," *IEEE Trans. Instrum. Meas.*, vol. 55, no. 1, pp. 266–272, Feb. 2006.
- [40] M. Wagih, A. S. Weddell, and S. Beeby, "Omnidirectional dual-polarized low-profile textile rectenna with over 50% efficiency for sub- $\mu\text{W}/\text{cm}^2$  wearable power harvesting," *IEEE Trans. Antennas Propag.*, early access, Oct. 20, 2020, doi: [10.1109/TAP.2020.3030992](https://doi.org/10.1109/TAP.2020.3030992).
- [41] V. Palazzi *et al.*, "A novel ultra-lightweight multiband rectenna on paper for RF energy harvesting in the next generation LTE bands," *IEEE Trans. Microw. Theory Techn.*, vol. 66, no. 1, pp. 366–379, Jan. 2018.
- [42] A. Okba, A. Takacs, and H. Aubert, "Compact rectennas for ultra-low-power wireless transmission applications," *IEEE Trans. Microw. Theory Techn.*, vol. 67, no. 5, pp. 1697–1707, May 2019.
- [43] S.-E. Adami *et al.*, "A flexible 2.45-GHz power harvesting wristband with net system output from -24.3 dBm of RF power," *IEEE Trans. Microw. Theory Techn.*, vol. 66, no. 1, pp. 380–395, Jan. 2018.
- [44] G. Monti, L. Corchia, and L. Tarricone, "UHF wearable rectenna on textile materials," *IEEE Trans. Antennas Propag.*, vol. 61, no. 7, pp. 3869–3873, Jul. 2013.
- [45] M. Pinuela, P. D. Mitcheson, and S. Lucyszyn, "Ambient RF energy harvesting in urban and semi-urban environments," *IEEE Trans. Microw. Theory Techn.*, vol. 61, no. 7, pp. 2715–2726, Jul. 2013.
- [46] C. Song, Y. Huang, J. Zhou, J. Zhang, S. Yuan, and P. Carter, "A high-efficiency broadband rectenna for ambient wireless energy harvesting," *IEEE Trans. Antennas Propag.*, vol. 63, no. 8, pp. 3486–3495, Aug. 2015.
- [47] C. Song *et al.*, "A novel six-band dual CP rectenna using improved impedance matching technique for ambient RF energy harvesting," *IEEE Trans. Antennas Propag.*, vol. 64, no. 7, pp. 3160–3171, Jul. 2016.
- [48] K. Mimis, D. R. Gibbins, S. Dumanli, and G. T. Watkins, "The ant and the elephant: Ambient RF harvesting from the uplink," *IET Microw. Antennas Propag.*, vol. 11, no. 3, pp. 386–393, Feb. 2017.
- [49] J. W. Matiko, N. J. Grabham, S. P. Beeby, and M. J. Tudor, "Review of the application of energy harvesting in buildings," *Meas. Sci. Technol.*, vol. 25, no. 1, 2014, Art. no. 012002.
- [50] D. Balsamo, O. Cetinkaya, A. R. Arreola, S. C. B. Wong, G. V. Merrett, and A. S. Weddell, "A control flow for transiently powered energy harvesting sensor systems," *IEEE J. Sensors*, vol. 20, no. 18, pp. 10687–10695, Sep. 2020.
- [51] C. R. Valenta and G. D. Durgin, "Harvesting wireless power: Survey of energy-harvester conversion efficiency in far-field, wireless power transfer systems," *IEEE Microw. Mag.*, vol. 15, no. 4, pp. 108–120, Jun. 2014.



**MAHMOUD WAGIH** (Graduate Student Member, IEEE) received the B.Eng. degree (Hons.) from the University of Southampton in 2018, where he is currently pursuing the Ph.D. degree.

In 2017, he worked as a Research Assistant with the University of Southampton, investigating novel differential transmission lines. In 2018, he was a Hardware Engineering Intern, and in 2020, as a Research Intern with Arm, Cambridge, U.K. His current research interests lie in RF energy harvesting, wireless power transfer, wearable antennas, in addition to printed microwave electronics. He has over 25 journal and conference publications and has delivered an invited webinar on these topics.

Mr. Wagih was the recipient of the Best Undergraduate Project Prize at the University of Southampton in 2018, and was selected for the IEEE International Microwave Symposium Project Connect in 2019. He received the Best Student Paper Award at the IEEE Wireless Power Transfer Conference in 2019, and the Best Oral Paper at PowerMEMS in 2019. He won the Best 3MT Presentation Prize (Second Place) at the IEEE Microwave Week in 2020. He has acted as a Reviewer for the IEEE TRANSACTIONS ON ANTENNAS AND PROPAGATION, IEEE SYSTEMS JOURNAL, IEEE SENSORS LETTERS, and SENSORS (MDPI).



**ALEX S. WEDDELL** (Member, IEEE) received the M.Eng. degree (Hons.) and the Ph.D. degree in electronic engineering from the University of Southampton, U.K., in 2005 and 2010, respectively.

He is currently a Lecturer with the Center for Internet of Things and Pervasive Systems, University of Southampton, and is involved with three projects funded by EPSRC, EU Horizon 2020 and Clean Sky 2. He has over 14 years' experience in design and deployment of energy

harvesting systems, and has published around 55 peer-reviewed papers in the area. His main research focus is in the areas of energy harvesting and energy management for future Internet of Things devices.



**STEVE BEEBY** (Senior Member, IEEE) received the B.Eng. degree (Hons.) in mechanical engineering and the Ph.D. degree in MEMS resonant sensors from the University of Portsmouth, Portsmouth, U.K., in 1992 and 1998, respectively.

He is currently the Head of the Smart Electronic Materials and Systems Research Group, University of Southampton, and leads the U.K.'s E-Textiles Network. He is currently leading three U.K. funded research projects and has received over £16 million research funding. He is a Co-Founder of Perpetuum Ltd., Southampton U.K., a University spin-out based upon vibration energy harvesting formed in 2004, Smart Fabric Inks Ltd., and D4 Technology Ltd. He has coauthored/edited four books, including *Energy Harvesting for Autonomous Systems* (Artech House, 2010). He has given 25 invited talks and has over 300 publications and ten patents. He has an H-Index of 52. His current research interests focus on energy harvesting, E-textiles and the use of energy harvesting in wearable applications.

Dr. Beeby was the recipient of two prestigious EPSRC Research Fellowships to investigate the combination of screen-printed active materials with micromachined structures and textiles for energy harvesting and was also awarded a Personal Chair in 2011. He is currently the Chair of the International Steering Committee for the PowerMEMS Conference series.